Saudi Journal of Biological Sciences 27 (2020) 2499–2508

Contents lists available at ScienceDirect

Saudi Journal of Biological Sciences

journal homepage: www.sciencedirect.com

Original article

Composites with alginate beads: A novel design of nano-adsorbents impregnation for large-scale continuous flow wastewater treatment pilots

Faissal Aziz [a,b,*], Mounir El Achaby [c], Amina Lissaneddine [a,b], Khalid Aziz [d], Naaila Ouazzani [a,b], Rachid Mamouni [d], Laila Mandi [a,b]

[a] Laboratory of Hydrobiology, Ecotoxicology, Sanitation & Global Changes (LHEAG, URAC 33), Semlalia Faculty of Sciences, Cadi Ayyad University, Marrakech, Morocco
[b] National Centre for Research and Study on Water and Energy (CNEREE), Cadi Ayyad University, Marrakech, Morocco
[c] Materials Science and Nano-engineering (MSN) Department, Mohammed VI Polytechnic University (UM6P), Benguerir, Morocco
[d] Materials, Catalysis and Valorization of Natural Resources, Faculty of Sciences, University Ibn Zohr, BP 8106, Agadir, Morocco

ARTICLE INFO

Article history:
Received 11 September 2019
Revised 10 November 2019
Accepted 18 November 2019
Available online 25 November 2019

Keywords:
Sodium alginate
Nano-adsorbents encapsulation
Cadmium(II)
Fixed-bed column

ABSTRACT

The sorption capacity of cadmium (Cd (II)) on three new generated nanocomposite beads sodium alginate (SA) based; SA-Clay (SA-C) beads, SA-Phosphate (SA-P) beads, and SA- Activated Charcoal (SA-Ch) beads was investigated in a batch scale, then a continuous flow reactor.

The highest adsorption capacity (137 mg/g) was obtained for SA-Ch using 1000 mg/L of initial Cd (II). The isotherm results showed that the adsorption equilibrium is compatible with the Langmuir isotherm and the sorption capacity of SA-Nano-adsorbent beads is very high. The models used for representing kinetic data was given that the removal of Cd (II) be well-fitted by second-order reaction kinetics. For the fixed bed column treatment, the maximum breakthrough times were 30, 38, and 48 h respectively for the SA-C, SA-P, and SA-Ch.

According to the obtained results, it was concluded that SA-Nano-adsorbent bead is an excellent designed material as a nanocomposite for cadmium elimination from wastewater in a continuous treatment process.

© 2019 The Author(s). Published by Elsevier B.V. on behalf of King Saud University. This is an open access article under the CC BY-NC-ND license (http://creativecommons.org/licenses/by-nc-nd/4.0/).

1. Introduction

In the last decades, many processes as ozonation, filtration by the membrane, precipitation, coagulation, reverse osmosis, and ion exchange have been applied for the elimination of pollutants from contaminated water (Zhou and Smith, 2002). However, these technologies have many disadvantages, since they often imply high costs because demand much energy and can carry on the formation of free radicals and sometimes more toxic than the initial pollutant (Wenzel et al., 2008).

By involving efficient and low-cost technology of micropollutants removal, the treated wastewater can be made available for re-use in different sectors (Aziz et al., 2013). Adsorption is an effective technique used in industry for heavy metals elimination (Aksu, 2001). It is a term commonly used for various processes comprise physical as well as chemical interactions between the solid surfaces of an adsorbent and dissolved metal ions. Adsorption allowing the treatment waters gives rise to a very rich bibliography through a very great variability of adsorbents.

The major economic constraint is often the cost of the selected material, the tested materials range from agricultural waste (Antunes et al., 2012; Bhatnagar and Sillanpää, 2010) to mineral ones (Aziz et al., 2016) for what can be considered as low-cost adsorbents. Other studies use modified materials (Avila et al., 2014) which are very expensive and therefore unusable on an industrial scale despite promising treatment yields. Recently, widen importance has been accorded on the biological materials' research as adsorbents for the elimination of pollutants, which might minimize the process price substantially and carry out the adsorption method more ecological and feasible.

* Corresponding author at: Laboratory of Hydrobiology, Ecotoxicology, Sanitation and Global Changes (LHEAG, URAC33), Faculty of Sciences Semlalia, Marrakech, Morocco.
E-mail address: faziz@kth.se (F. Aziz).

Peer review under responsibility of King Saud University.

Production and hosting by Elsevier

https://doi.org/10.1016/j.sjbs.2019.11.019
1319-562X/© 2019 The Author(s). Published by Elsevier B.V. on behalf of King Saud University.
This is an open access article under the CC BY-NC-ND license (http://creativecommons.org/licenses/by-nc-nd/4.0/).

Actually, nano-particles have been applied for their ability as adsorbents (Aziz et al., 2016). Their smaller dimension increases their specific surface (Gubin et al., 2005) that improves their chemical response and adsorption potential to fix pollutants (Kalfa et al., 2009).

At present, the inadequacy of adsorption purification systems on an industrial scale has, therefore, waken a very dynamic area of investigation into the implementation of innovative processes that make it possible to improve purification yields. The transition from the experimental scale to the implementation of techniques on industrial facilities was often constrained by economic or practical reasons.

This confirms the effectiveness of nano-materials using in water purification; however, this method has some disadvantages, such their ability to be released into the environment in preparation and purification procedure, which could cause serious environmental and health problems, those downsides should be well-respected during the design of a new form of nano-particle applications (Bundschuh et al., 2018).

In this sense, generation of composites is a new method to fix those nano-adsorbents in a rigorist form by embedding it in rigid support such as a synthetic or natural polymer (Aziz et al., 2016). This technique has many advantages, in first it guaranteed the nanoparticles trap and get it very difficult to release it in the environment, which we can control their reutilization by regeneration the nano-composites in a whole that give also the possibility to recover the adsorbate for later use. Another advantage is that the method facilitates the transfer of the batch adsorption process to fixed-bed column because the continuous flow treatment pilots are the demanded form in the large-scale application.

Alginate beads are regular backing materials in many technologies (Matricardi et al., 2008) and recently are applied for the environmental remediation (Escudero et al., 2006; Silva et al., 2008). Sodium alginate is differing from many other biopolymers and extracted from brown algae and bacteria (Painter, 1983; Gorin and Spencer, 1966). It is a copolymer of two epimer uronic acids: 1,4-(b-D)- mannuronic acid (M) and 1,4-(a-L)-guluronic acid (G). This polymer is biocompatible, low cost and efficient encapsulating technique (Scott et al., 1989).

The wastewater treatment operation at the real scale requires granular materials of controlled size, which numerous researcher had to generate those materials by the encapsulation of diverse adsorbents in the alginate composite to improve their potentials (Escudero et al., 2006, 2009; Ngomsik et al., 2006; Bhat and Aminabhavi, 2006).

In order to put directly the adsorption technology for real-scale applications in wastewater purification, it's necessary to carry out continuous flow studies using a column model to assess the intended contact time which the adsorbate attain an equilibrium.

In this work, the sorption properties have been made through encapsulation with alginate of nano-adsorbent selected from three natural materials (Moroccan Clay, phosphate rock and marble powder waste) compared to the activated carbon material, to remove cadmium (Cd) in a fixed bed column and reach the design parameters of adsorption in this process of continuous treatment.

2. Materials and methods

2.1. Materials and chemicals used in experiments

Sodium Alginate SA (analytical grade, viscosity (1%; 20 °C) was purchased from PanReac AppliChem. Calcium chloride anhydrous ($CaCl_2$) which were used for preparation of beads and Cadmium nitrate $Cd(NO_3)_2$ to prepare a stock solution of 1000 mg. Both products were supplied by Sigma-Aldrich.

2.2. Generation of beads

The procedure for the preparation of alginate beads production was based on the cross-linking process. 2 g of the SA was melted in 100 mL of distilled water to generate a slimy solution after agitation at 25 °C. The solution is introduced drop by drop, under magnetic stirring, using a syringe into 100 mL of 20 g/L $CaCl_2$ solution using a 10 mL syringe.

SA-Clay (SA-C) beads, SA-Phosphate (SA-P) beads, and SA-Activated Charcoal (SA-Ch) beads are prepared as following 10 g of natural clay, natural phosphate, and activated charcoal respectively, then were put within SA solutions during two hours of agitation in order to make a homogeneous dispersion. The mixture's solutions were dropped in a solution of $CaCl_2$.

The solutions were confined in the umbra to solidify (24 h). The encapsulated beads were then immersed in distilled water, several times and kept in distilled water, the average size of those beads is 2 mm. The process of bead composites production is shown in Schematic 1.

2.3. Characterization of beads

Scanning electron microscopy (SEM, VEGA3 TESCAN) was utilized to get the qualitative properties of the physical organization and the morphology of SA beads, SA-C beads, SA-Pbeads, and SA-Ch beads. Using an energy-dispersive X-ray spectroscopy (EDX) analyzer TEAM™ EDS to measure elements in micro-area and the condition of elements distribution in the beads.

Fourier transform infrared spectroscopy was used to characterize the chemical structures of the beads. The FTIR spectra were measured on a VERTEX 70 infrared spectrometer using the KBr powder to produce pellets by compression in the wavelength range of 500–4000 cm^{-1}.

The proprieties of materials in terms of arrangement and composition were achieved by X-ray diffraction (XRD) diagrams with monochromatic. The results were gotten with the diffraction angle (2θ) from 10° to 80°.

The specific surface (S_{BET}) was measured by the Brunauer, Emmett and Teller (BET) method. The pore size distribution (0.50–249 nm) is obtained utilizing a finite slit pore model (Jagiello and Olivier, 2013) simulated by NLDFT (Non-Linear Density Functional Theory) and applied to the adsorption isotherm from N_2 to 77 K. In the ultra-micropore range, the distribution (0.33–0.80 nm) is obtained by a DFT simulation with an infinite slit pore model (Jagiello and Thommes, 2004) of the CO_2 adsorption isotherm at 273 K.

2.4. Experiment

2.4.1. Cadmium adsorption in a batch system

Adsorption isotherms were investigated by adding 10 g of nanocomposite beads of Clay beads, SA-Phosphate beads and SA-Charcoal into 100 mL of synthetic solutions of 500 mg/L Cd (II). In another side, 1 g of the raw material of each adsorbent into 100 mL of the same solution to be treated.

The initial pH values of the solution were 7 and experiments were studied at room temperature. After the suspensions were shaken for 4 h in an automatic incubator (Model: HEIDOLPH UNIMAX 2010) shaker, then the samples were collected at various intervals of time (30 min). The remaining quantity of Cd (II) was

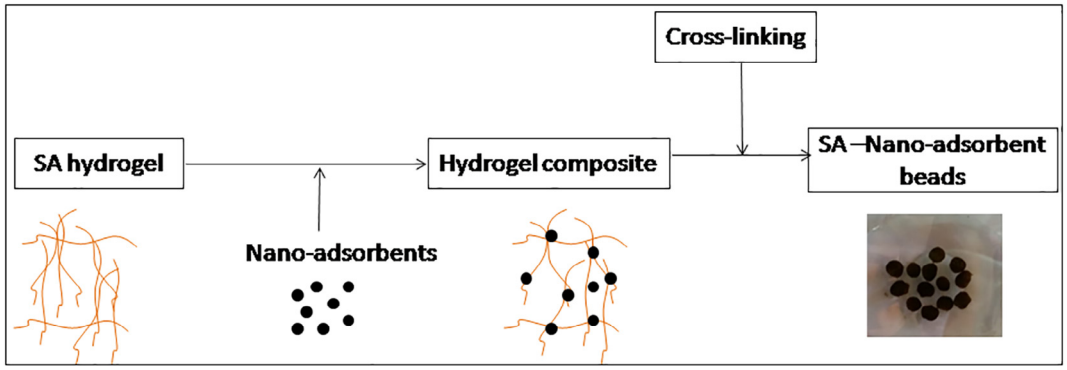

Schematic 1. Schematic representation the preparation of SA–Nano-adsorbent.

measured utilizing the Atomic Absorption Spectrometer (Model: SHIMADZU AA 6300).

The equilibrium adsorption capacity (q_e, mg/g) was obtained using Eq. (1):

$$q_e = \frac{(C_0 - C_e) \times V}{m} \quad (1)$$

where V is the volume of the solution (mL) and m is the mass of adsorbent (mg). C0 is the initial Cd (II) concentrations; Ce is the Cd (II) quantity after adsorption test (mg/L).

2.4.2. Adsorption isotherms

In the aim to establish the correlation among the adsorbed cadmium ion quantity and the remaining ions in the solution, the adsorption isotherm investigation was achieved at equilibrium. The obtained data were integrated into both the Langmuir and Freundlich isotherm models.

The Langmuir model supposes that the adsorption of metal ions presents as a monolayer on a homogeneous surface and the non-linear equation is written as:

$$q_e = \frac{q_m K_L C_e}{1 + K_L C_e} \quad (2)$$

where:

K_L = Langmuir equilibrium constant (L/mg).

q_m = the quantity of adsorbate (mg) necessary to fill all the accessible sites in adsorbent (g).

C_e = the equilibrium concentration (mg/l).

The Freundlich isotherm model is envisaged to be relevant for depicting sorption on heterogeneous surfaces and multilayer sorption. The Freundlich is expressed by the Eq. (3):

$$q_e = K_f Ce^{1/n} \quad (3)$$

where q_e is the adsorption capacity in mg/g at equilibrium, C_e the concentration at the equilibrium of metal in mg/L, K_f the constant linked to the adsorption capacity, and n the empirical constant related to the adsorption capacity.

2.4.3. Kinetic studies

To study the mechanisms commanding batch adsorption and to upgrade describe the behavior of the generated nano-adsorbents, the adsorption results were analyzed utilizing the pseudo-first-order, and the pseudo-second-order using Eqs. (4) and (5):

$$\log(q_e - q_t) = \log q_e - \frac{K_1 t}{2.303} \quad (4)$$

$$\frac{t}{q_t} = \frac{1}{K_2 q_e^2} + \frac{t}{q_t} \quad (5)$$

where q_e and q_t are the quantity of metals removed (mg/g) at equilibrium and at time t (min), k_1(min^{-1}) and k_2 (g mg^{-1} min^{-1}) are the adsorption ratio constant, respectively of pseudo-first-order and pseudo-second order adsorption rate.

2.4.4. Cadmium adsorption in a continuous fixed-bed column system

In this study, the continuous system tests were realized in a glass column with an inner diameter of 5 cm and a height of 40 cm. 150 g of nano-adsorbents beads with average diameters of 2.5 mm was packed into the column. The Cd(II) solution (500 mg /l) was passed down into the bottom of the column by a peristaltic pump at a constant flow rate of 2 mL/min.

The quantity of the cadmium (II) in solution was determined at specific time intervals and obtained by Atomic Absorption Spectrometer (SHIMADZU: AA type 6300/GFA-EX7i).

The treated solution was collected every hour until the breakthrough curve was obtained.

3. Results and discussion

3.1. Characterization of the beads

3.1.1. Fourier transform infrared spectroscopy

Fourier transform infrared spectroscopy (FTIR) is an extensive method that is usually used to analyze materials (Rehman and Bonfield, 1997). It can provide for the determination of types and intensities of their surface functional groups.

The FTIR spectrum of SA beads, SA-Clay beads, SA-Phosphate beads, and SA-Charcoal beads are compared in Fig. 1.

The SA beads FTIR spectra exhibits the peaks around 3429, 1628, 1428, and 1031 cm^{-1}, designating respectively the elongation of O–H, COO–(asymmetric), COO– (symmetric), and C–O–C, (Puttipipatkhachorn et al., 2005).

Fig. 1 indicates a wide peak at 3441, 3418 and 4317 cm^{-1} is assigned to OH functions, and small variation was spotted in OH peak stretching after mixing alginate respectively with clay, phosphate and Charcoal. The band at 2925, 2515 and 2377 cm^{-1} in the spectra SA-Clay beads, SA-Phosphate beads, and SA-Charcoal beads respectively are assigned to the CH extension vibration from glucose molecules in alginate (Ely et al., 2011). The bands at 1637, 1626, 1603 cm^{-1} and 1427, 1429, 1415 cm^{-1} showed in the peak are respectively assigned to the asymmetric and symmetric elongate bands of COO of the alginate molecule.

For SA-Clay beads FTIR spectra, the elongate band characterizes the vibration of SiO was showed at 1019 cm^{-1}. The absorption band at a low frequency at 578 cm^{-1} from SiOAl (Oladipo and Gazi, 2014).

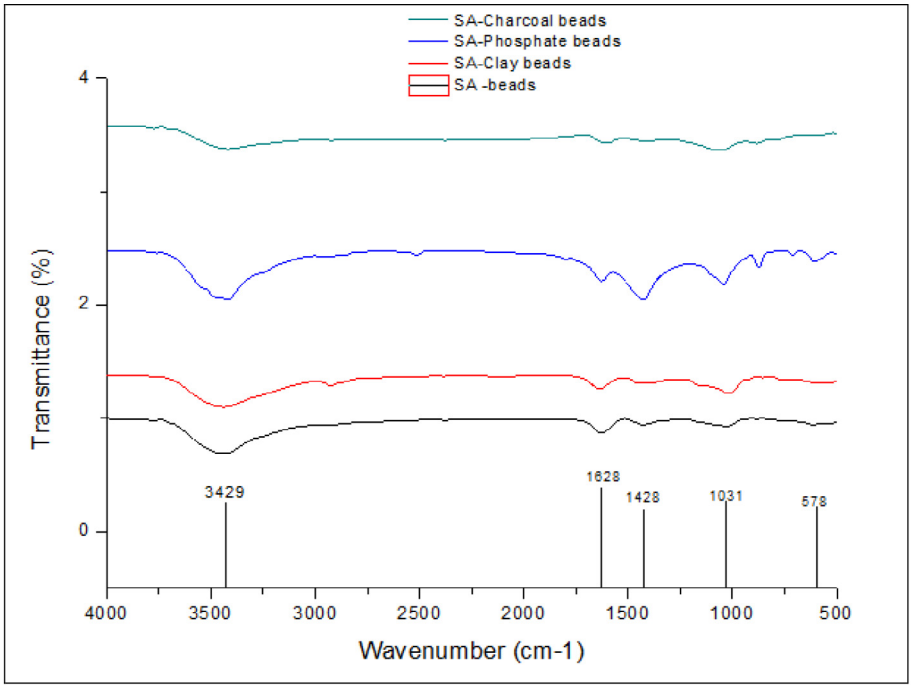

Fig. 1. FTIR of SA beads, SA-Clay beads, SA-Phosphate beads and SA-Charcoal beads.

The FTIR spectra of SA-phosphate beads, for which the IR peaks assigned to PO_4^{3-} valence linking forms are shown at 1140 cm^{-1} (Salah et al., 2006).

The results reveal the lack of any chemical reaction between alginate and materials (clay, phosphate, charcoal) besides the breakage of hydrogen bonds during the processes of dissolution and regeneration.

Taken into consideration the results of the FITR spectra, composite beads were obtained by hydrogen liaison and thermal action before cross-linking.

3.1.2. SEM analysis

SEM can amplify the object 100,000 times. It is useful to better comprise the micromorphology on the solid surface and measure the fractured state of materials. The micrographs SA beads, SA-C beads, SA-P beads, and SA-Ch beads were observed and are shown in Fig. 2.

Alginate and $CaCl_2$ are capable to establish a hard structure, according to his successive emplacement of G units on alginate which generate hollow to calcium ions to join, which every ion capable to link to four G units. The design represents the ionotropic gelation of alginate and is named as the "egg-box" model (Draget et al., 2003; Thu et al., 1996).

According Fig. 2(a) SA beads had a rough and lacunar surface with large wrinkles. Whereas the composite beads (SA-C beads, SA-P beads and SA-Chbeads (Fig. 2(b)–(d)) have a rugged surface due to the cavity, which generated over the cross-linking operation. The shape of composite beads can be described as spherical.

The porous surface organization ought to be considered as an agent affording an expansion in the specific surface and the permeability of composite beads. Moreover, these cavities facilitate the pore diffusion during adsorption due to the importance of the inner specific surface with a weak diffusion resistance in the composite beads (involve advanced adsorption potential and rate). Porous nature is clearly evident from this micrograph.

3.1.3. EDX analysis

The EDX characterization was achieved. It allows to quantifying the active molecules preserved in the beads. The EDX analysis of SA beads, SA-Clay beads, SA-Phosphate beads, and SA-Charcoal beads are shown in Fig. 3.

Sodium alginates are the sodium salt of alginic acid which its chemical composition is "$C_6H_9NaO_7$" (Thu et al., 1996). EDX analysis (Fig. 3(a)) marked that SA beads were principally composed of oxygen (54.91%), calcium (10.04%), chlorine (2.80%) and carbon (30.94%), also a small tracks of sodium (1.31%) which are results in conformity with the research of Ramos et al., 2018.

The beads are very analogous in view of their chemical structure, except the existence of aluminum that considered the most pertinent difference (0.65%) and silicon (0.03%) in SA-Clay beads, phosphorus (1.38%) and silicon (4.16%) in the SA-Phosphate beads and potassium (3.52%) and silicon (3.84%) in the SA-Charcoal beads. These results were logic due to the presence of clay, phosphate, charcoal respectively in beads.

As shown in Fig. 3, there were no other impurity peaks that appeared in EDX spectra. These are in conformity with results obtained before in the part of FTIR.

The presence of peaks of some phosphorus, aluminum, potassium and silicon molecules revealed that successful functionalization of the alginate was carried out when compared with the plain alginate elemental composition.

3.1.4. XRD analysis

The crystalline nature of SA beads, SA-C beads, SA-P beads, and SA-Chbeads was also analyzed by the XRD pattern. Fig. 4 presents the XRD patterns of bead samples in 2θ scan range of 10–90°.

XRD patterns of SA beads, SA-C beads, SA-P beads, and SA-Ch beads are given in Fig. 4. No diffraction peak was observed for SA beads indicating that this material is amorphous.

The XRD analysis of SA-Phosphate beads reveals the presence of the following phases: fluorapatite; $Ca_{10.00}P_{5.77}C_{0.08}O_{24.64}F_{1.84}$ (Reference code: 96-901-0505), quartz: $Si_{6.00}O_{6.00}$ (Reference code: 96-101-1160), carbonates-fluorapatite: $Ca_{4.04}P_{2.36}O_{17.66}F_{0.33}$

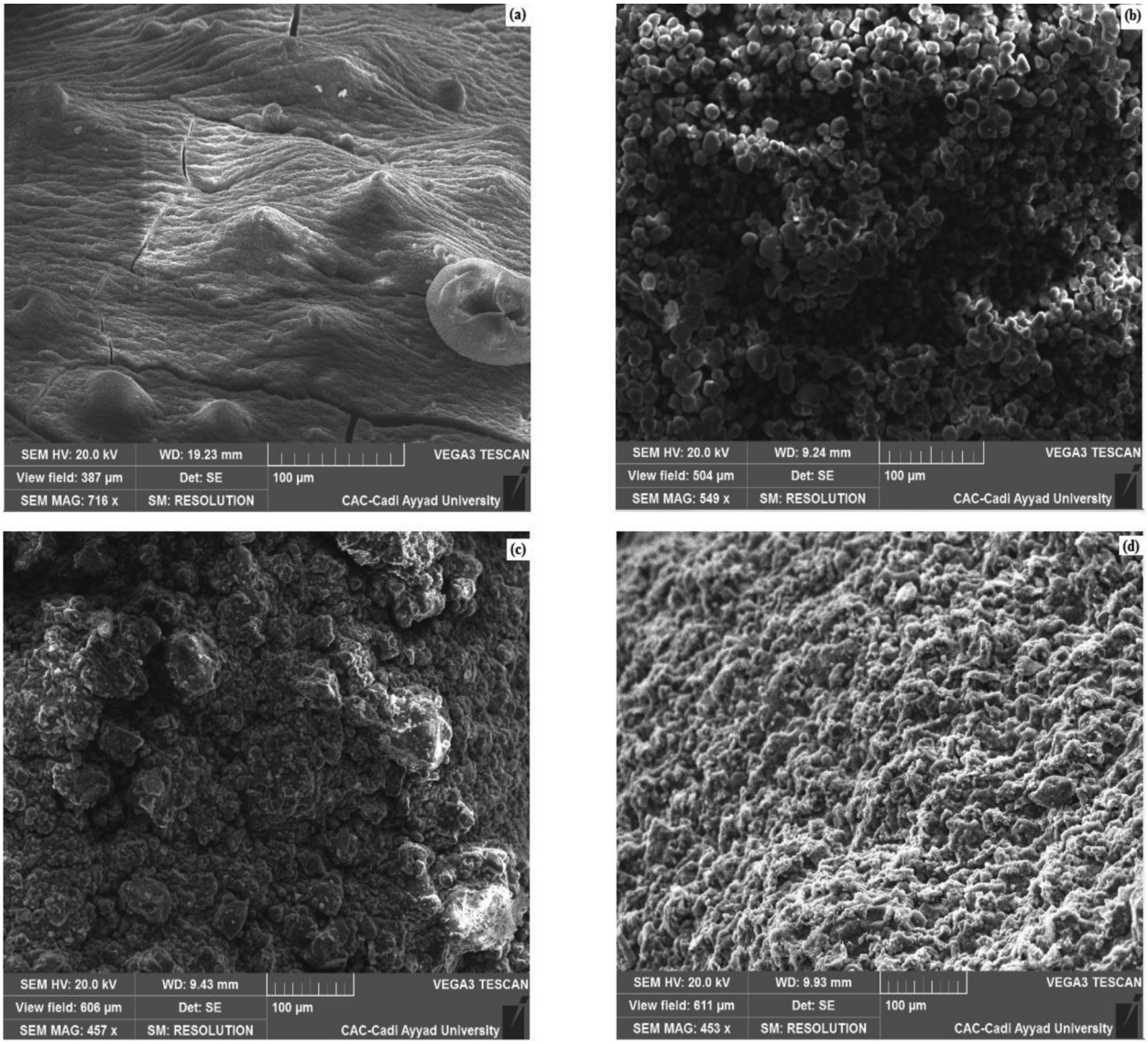

Fig. 2. SEM of SA beads (a) SA-Clay beads (b) SA-Phosphate beads (c) SA-Charcoal beads (d).

(Reference code: 96-900-9979) and calcite: $Ca_{6.00}C_{6.00}O_{18.00}$ (Reference code: 96-901-6707). The characteristic XRD signals of charcoal were detected in SA-Charcoal: Si O (2ϑ = 21.10, 12.87, 36.78, 39.49, 42.55, 50.30, 60.21, 68.15 and 75.90), which undoubtedly confirms that the encapsulation of phosphate and charcoal in the polymer at a molecular level, allow them to not re-crystallize in the particles.

The XRD pattern of SA-C beads showed characteristic peaks of SA-C beads, but with less intensity because of the intercalation of clay in the hydrogels SA which caused to increase the amorphous nature of the beads.

3.1.5. Textural analysis

The ability of alginate to form stable hydrogels considered one of the major characteristics, that promise for its ample industrial uses. The Table 1 indicates the specific surface area (SSA), pore volume, and size of the nanoadsorbent beads based on alginate sodium. The SSA of the SA-Ch composite was 389 m^2/g, which is high than the SA-P (291 m^2/g) and the SA-C (255 m^2/g). This probably related to the difference of the surface area between the tested composites and the cross-linking behavior of those nanomaterials with alginate during the encapsulation step.

In this part of texture characterizations, we point out also the differences between these microporous nanocomposites alginate-based, this determination of the three porosity form gave enough information concerning the amount of porosity and the quantity of pore widths. The elevated SBET surface area is a sign of the presence of an important microporosity. The results showed that compared to the beads of sodium alginate only, SA- Ch and SA-P present a higher volume of narrower micropores, while SA-C has a higher percentage of larger micropores.

Thus, we suppose the production of ultra micro pores and super micro pore over the adsorbent encapsulation and these pore structures became dense with cross-linking nanoadsorbents in alginate. The hydrogel of alginate had potential to immobilize many materials and might generate materials of controlling form, waist, and porosity produces it an encouraging tool as an adsorbent.

3.2. Cadmium uptake capacity of various alginate bead composites

Cadmium was picked as a model of heavy metal and the cadmium adsorption capacity of diverse alginate polymer-based adsorbents was tested. The equilibrium adsorption isotherms

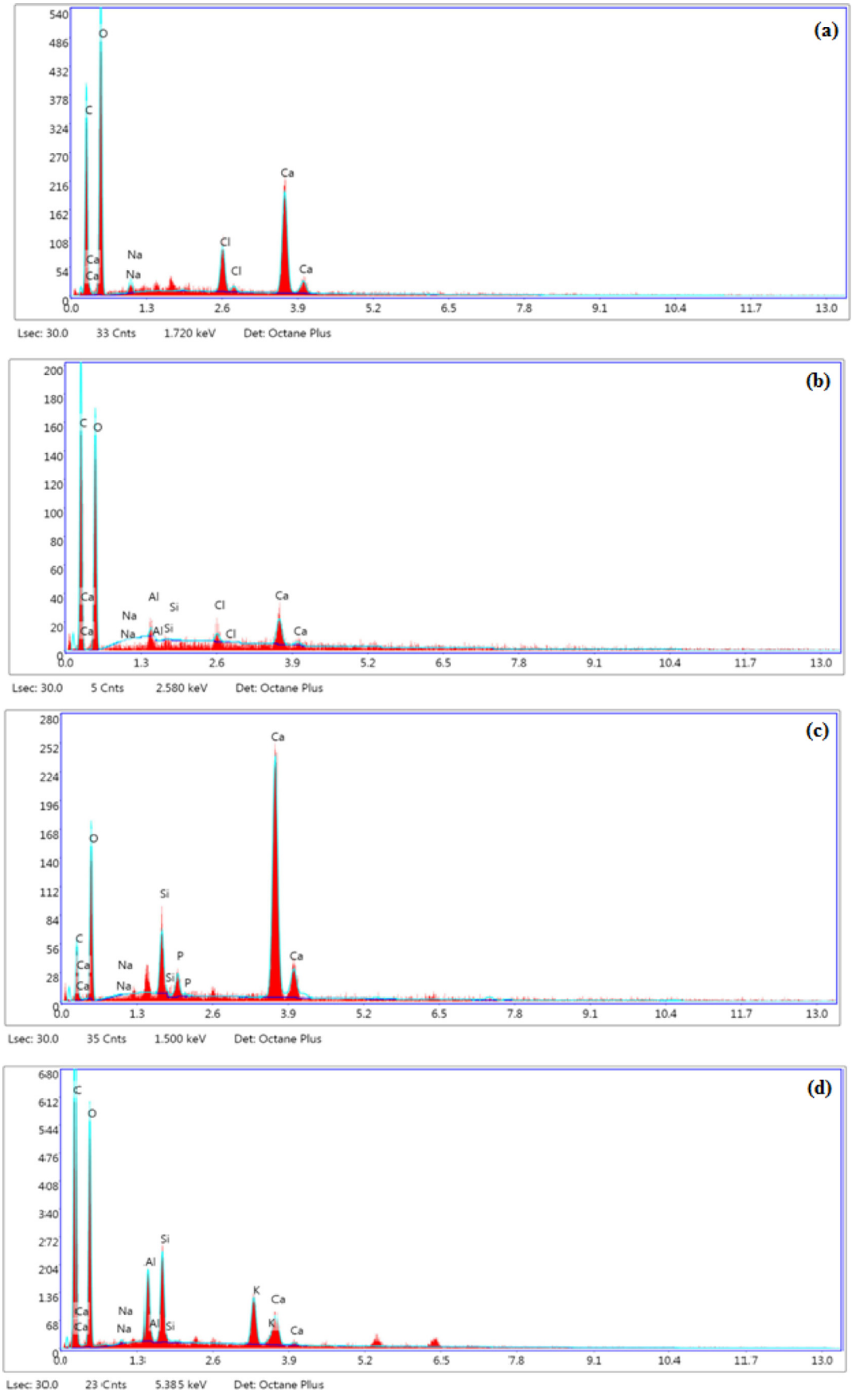

Fig. 3. EDX of surface of SA beads (a) SA-Clay beads (b) SA-Phosphate beads (c) SA-Charcoal beads (d).

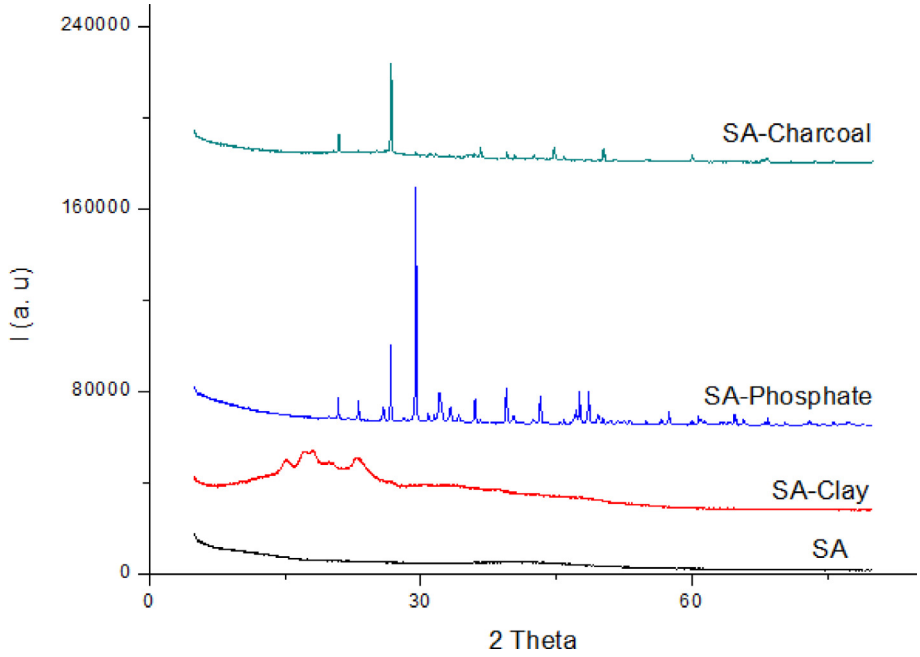

Fig. 4. X-ray patterns of the SA beads, SA-Clay beads, SA-Phosphate beads and SA-Charcoal beads.

Table 1
Textural characterization of alginate bead composites.

Beads	Texture			
	Specific surface area BET (m^2/g)	Volume of the ultra-micropores (0,2 to 0,8nm) (cm^3/g)	Volume of the Super-micropores (0,8 to 2 nm) (cm^3/g)	Volume des Meso-pores (2 à 50 nm) (cm^3/g)
SA	4.1	0	0.06	0.11
SA-C	255	0.09	0.12	0.19
SA-P	291	0.23	0.24	0.08
SA-C	389	0.21	0.19	0

represent the interaction between the material and the ionic metal. These isotherms are a tool for the optimization of the removal process and the loading ability of the adsorbent. The initial Cd(II) metal concentration action on adsorption was investigated to assess the maximum loading capacity of the generated bead composites of SA-C, SA-P, and SA-C.

According to Fig. 5, the adsorption abilities of Cd(II) onto the tested bead composites were classified as: SA-Ch > SA-C > SA-P. Such discordance could due to the structure characteristics of the bead composites (such as BET-SAA and pore dimensions, see Table 1). As indicated too, the SA-Ch nanoadsorbent beads showed the highest SSA-BET and porosity and also reached the highest adsorption potential. However, the SA-P presented the undermost SAA and porosities with the lowest adsorption potential. These results are in harmony with other studies in pervious works which consider the material structure characteristics, as a significant parameters for achieving a raised sorption capacity (Kasperiski et al., 2018; Umpierres et al.,2018).

The experimental data were analyzed using non-linear equations of most commonly used isotherm models such as Langmuir and Freundlich. A plot of Ceq/qe vs. Ceq and of log qe vs. log Ceq

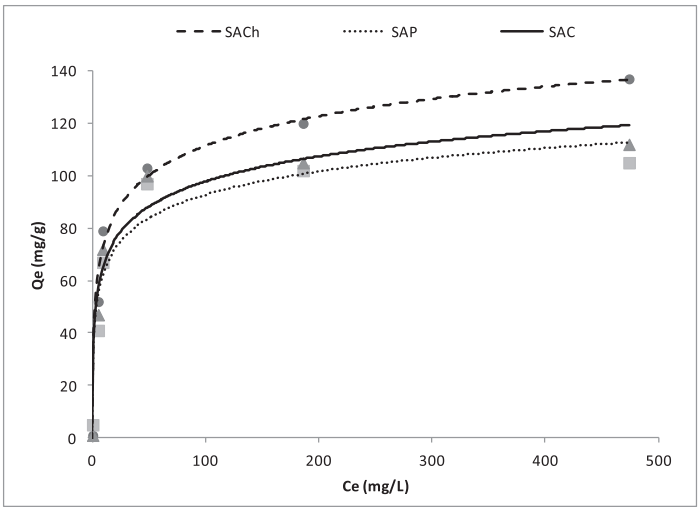

Fig. 5. Adsorption capacity of SA-Clay beads, SA-Phosphate beads and SA-Charcoal beads as a function of equilibrium concentration of Cd(II).

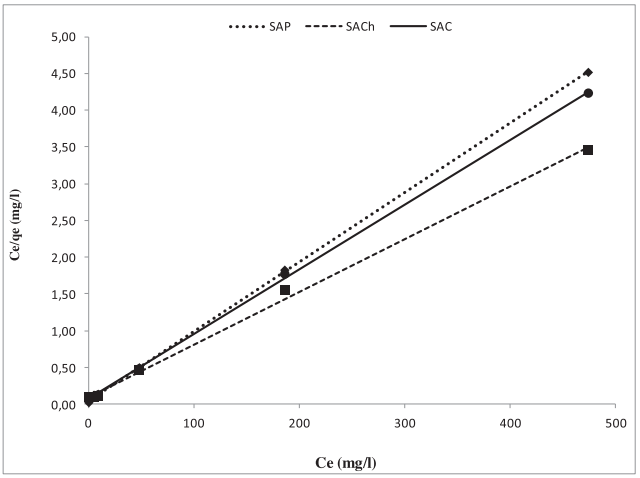

Fig. 6. A plot of Ceq/Cads vs Ceq confirming the applicability of the Langmuir adsorption isotherm.

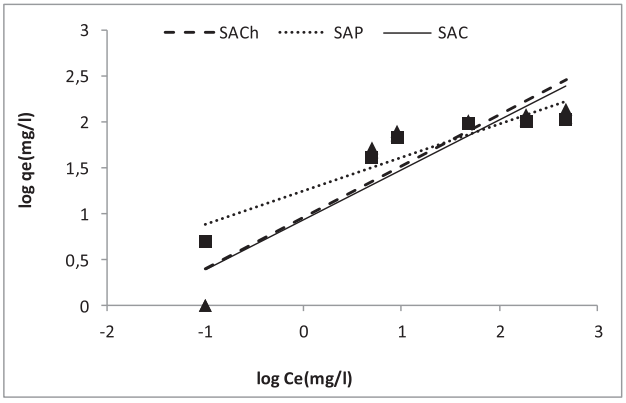

Fig. 7. Freundlich equation plots of log Cads vs. log Ceq yielded a straight line for the three Nano-adsorbent beads.

present a righteous line as shown in Figs. 6 and 7. The plots exhibited a good correlation coefficient and linearity that favors the use of Langmuir and Freundlich models in this work.

The results of Langmuir factors got from analyzing of the experimental data and the correlation coefficient (R^2) are presented in Table 2. The important R^2 value that are very close to the unit, marked that the adsorption results are compatible with Langmuir model and the adsorption of Cd(II) suitably undergo a monolayer and homogeneous adsorption mechanism. Even that, according to the Freundlich adsorption model, the n values are in the range 1–10 which indicate the most excellent adsorption and a propitious physical process, and the higher values of K_f mean an excellent adsorption aptitude.

The batch adsorption mechanism evolution was explored using the pseudo-first-order, and the pseudo-second-order. The pseudo-first order model envisages that the percentage of adsorption sites saturation is correlated to the amount of vacant sites.

The results of K_1 and qe were gotten basing on the slope and intercept of the linear plot of log ($q_e - q_t$) versus t (Fig. 8). The regression coefficient (R^2) results noted a modest convenient to the adsorption mechanism (Table 3). However, the pseudo-second order model that considered the hypothesis which adsorption proceeds a second-order chemisorption showed a higher value R^2 for SA-Ch. This implies that chemisorptions are not the main process for the sorption of Cd(II) ionic metals unto SA-Ch. The results of K_2 and q_e were gotten from the slope and intercept of the linear plot of t/q_t versus t (Fig. 9).

Concerning the treatment by a fixed column bed, the results of the concentration-time profile (breakthrough curve) are

Table 2
The isotherm model parameters of Alginate Nanocomposites beads.

	Langmuir isotherm				Freundlich isotherm		
	qmax (mg.g-1)	KL (L.mg-1)	b (L.mg-1)	R^2	Kf (L.mg-1)	n	R^2
SA-C	112	0,570	0,0754	0,9996	8,732	1,8416	0,8095
SA-P	105	0,669	0,0494	0,9978	17,873	2,7563	0,8773
SA-Ch	137	0,501	0,0996	0,9996	9,097	1,7803	0,822

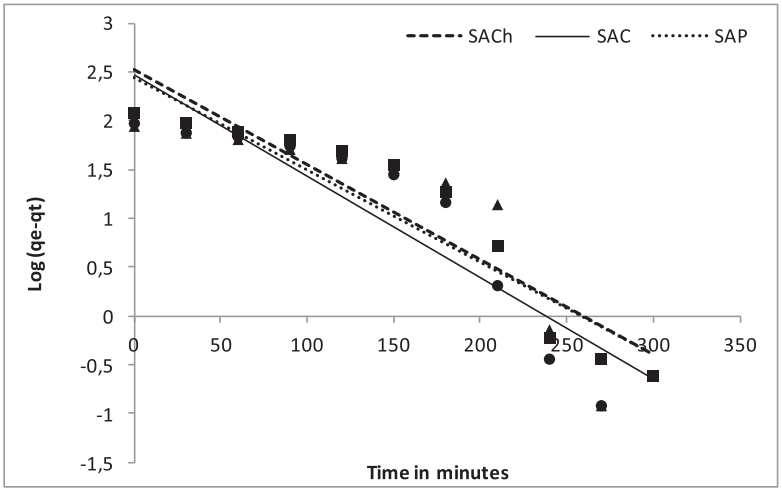

Fig. 8. Pseudo first- order equation plot of SA-Clay beads, SA-Phosphate beads and SA-Charcoal beads.

Table 3
Kinetic models comparison for the elimination of Cd(II) applying Alginate Nanocomposites beads.

	Pseudo-first-order				Pseudo-second-order			
	qe,exp (mg/g)	qe,cal (mg/g)	k_1 (min^{-1})	R^2	qe,exp (mg/g)	qe,cal (mg/g)	k_2 10^{-5} (g/mg/min)	R^2
SA-C	93,6	291,47	0,02395	0,8667	93,6	256,41	2,677	0,71
SA-P	87,48	278,16	0,02187	0,7906	87,48	303,03	2,407	0,8471
SA-Ch	119,76	331,21	0,02233	0,7906	119,76	243,90	1,894	0,9406

represented in Fig. 10. The breakthrough curve is necessary for the conception of an adsorption column. The results mentioned that the breakthrough time for the adsorption of Cd (II) increase for SA-Ch than SA-P and SA-C. The maximum breakthrough times were 30, 38, and 48 h respectively for the SA-C, SA-P, and SA-Ch.

In applied processes at industrial scale, the adsorbent is mostly in the form of small particles in a fixed bed column. Practically, an industrial scale treatments of heavy metal removal from effluents are realized in continuous mode. A fixed-bed column is often to bring contaminated water into contact with the adsorbent.

The continuous flow treatment operation seems to have several advantages than batch process because rates of adsorption related to the concentration of the adsorbate in effluent being treated. For

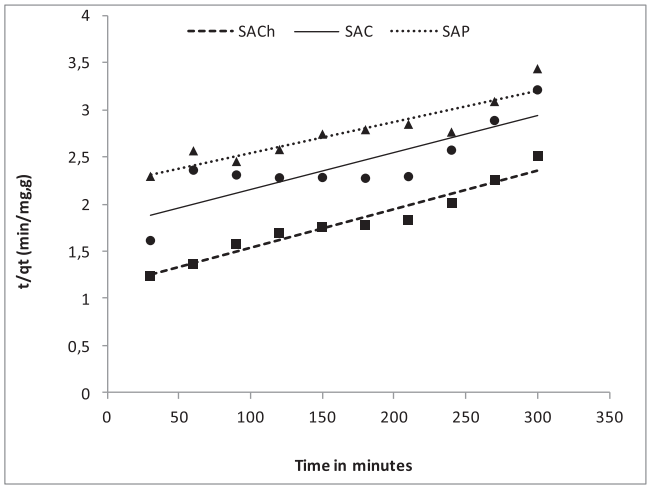

Fig. 9. Pseudo second- order equation plot of SA-Clay beads, SA-Phosphate beads and SA-Charcoal beads.

that continuous treatment process, we could add the solid adsorbents at the top of the column and remove the worn adsorbents from the bottom.

These results show the achievement of the feasibility of agglomerating the adsorbent nanoparticles into macroparticles by keeping these best adsorption capacity potentials in order to avoid clogging during the column treatment process. This new design promotes the industrial-scale application to treat effluents in a continuous flow which is the best practical way in the real application.

Though, many generated adsorbent particles have some inconveniences, as like production difficulty, poor adsorption potential and selectivity, prolonged equilibrium time, low stability and mechanical resistance and difficulty of their regeneration, etc., which reduce their capacity to use in batch and continuous process.

Whereof, it is obligatory to optimize easy, low cost and thrifty method for the production of new adsorption particles with admirable characteristics such as good adsorption capacity and selectivity, excellent resistance and regeneration, in particular, to have characteristics to perform column operation.

4. Conclusion

A variety of nano-particles have been generated and tested for contaminated water purification. These involve nano-adsorbents that have an efficient capacity to eliminate ionic metals. However, the most application of these adsorbents is their application for the static adsorption tests, while the convenient applications of real scale treatment systems require to utilize the continuous flow process.

In this study, we are followed a new approach to benefit from the capacity of those nano-adsorbents to be used in an applied sys-

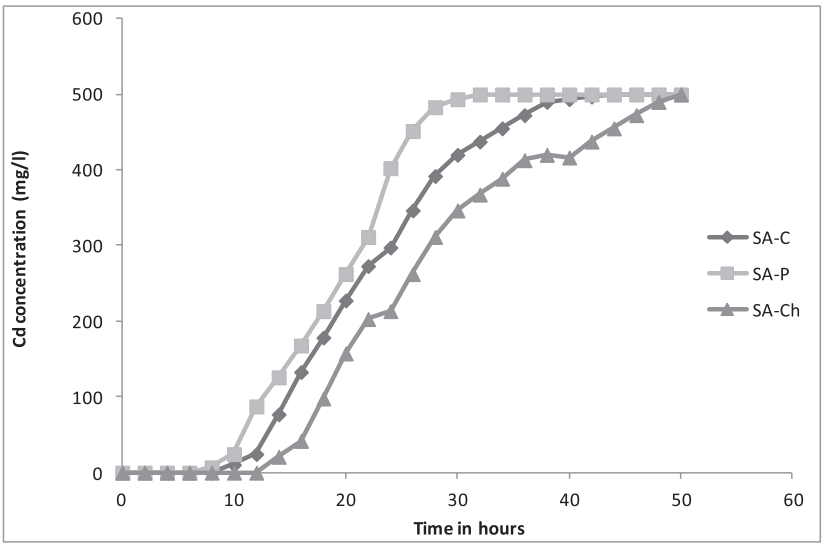

Fig. 10. The breakthrough curve of Cd (II) adsorption onto SA-Clay beads, SA-Phosphate beads and SA-Charcoal beads at 2 mL/min flow rate.

tem for purification. For that we generated granular particles with mastered dimension by the encapsulation of various nanoadsorbents in sodium alginate (SA) beads. Three materials of SA-Clay (SA-C) beads, SA-Phosphate (SA-P) beads, and SA- Activated Charcoal (SA-Ch) beads are prepared, characterized then tested adsorb the Cd (II) contained in an aqueous solution.

The XRD results afford justificatory proof to the FTIR data which some specific chemical interactions are made between sodium alginate and the tested nano-adosrbents. SEM images and BET analysis indicate a scabrous surface texture for the nanocomposite beads with umpteen pores.

The use of SA-Nano-adsorbent beads as an adsorbent for cadmium was investigated. This novel nanocomposites can eliminate cadmium metals from contaminated water. The experimental results are convenient to Langmuir and pseudo-second order models with high correlation factors. The pseudo-second order model neatly represents the adsorption mechanism of Cd (II) onto SA-P and SA-Ch beads in contrast to the result linked to the sorption of Cd onto SA-C beads.

The use of granulous materials based on alginate polymer as the adsorbent can be more studied involving of each constituent such as adsorbent and polymer, to remove all kind of pollutants from water. This will guide investigators to look for low-cost, efficient and eco-friendly adsorbents that have binding capacities to remove toxic pollutant compounds.

Acknowledgement

This work was supported by the MENARA project (Assessment of wastewater treatment technologies and promotion of smart irrigation systems in the MENA Region using an eco-friendly gum), DUPC2: IHE Delft Partnership Programme for Water and Development.

References

Aksu, Z., 2001. Equilibrium and kinetic modeling of cadmium(II) biosorption by C. vulgaris in a batch system: effect of temperature. Sep. Purif. Technol. 21, 285–294.

Antunes, M., Esteves, V., Guegan, R., Crespo, J., Fernandes, A., Giovanela, M., 2012. Removal of diclofenac sodium from aqueous solution by Isabel grape bagasse. Chem. Eng. Sci. 192, 114–121.

Avila, M., Burks, T., Akhtar, F., Göthelid, M., Lansåker, P., Toprak, M., Mamoun, M., Uheida, A., 2014. Surface functionalized nanofibers for the removal of chromium(VI) from aqueous solutions. Chem. Eng. J. 245, 201–209.

Aziz, F., Mandi, L., Boussaid, A., Boraam, F., Ouazzani, N., 2013. Quality and disinfection trials of consumption water in storage reservoirs for rural area in the Marrakech region (Assif El Mal). J. Water Health 11 (1), 146–160.

Aziz, F., Ouazzani, N., Mandi, L., Mamoun, M., Uheida, A., 2016. Composite nanofibers of polyacrylonitrile/natural clay for decontamination of water containing Pb(II), Cu(II), Zn(II) and pesticides. Sep. Sci. Technol. 52, 58–70.

Bhat, S.D., Aminabhavi, T.M., 2006. Novel sodium alginate-Na + MMT hybrid composite membranes for pervaporation dehydration of isopropanol 1,4-dioxane and tetrahydrofuran. Sep. Purif. Technol. 51, 85–94.

Bhatnagar, A., ans Sillanpää, M., 2010. Utilization of agroindustrial and municipal waste materials as potential adsorbents for water treatment—a review. Chem. Eng. J. 157, 277–296.

Bundschuh, M., Filser, J., Lüderwald, S., McKee, M.S., Metreveli, G., Schaumann, G.E., Schulz, R., Wagner, S., 2018. Nanoparticles in the environment: where do we come from, where do we go to?. Environ. Sci. Eur. 30, 6.

Draget, K.I., Stokke, B.T., Yuguchi, Y., Urakawa, H., Kajiwara, K., 2003. Small-angle X-ray scattering and rheological characterization of alginate gels. 3. Alginic acid gels. Biomacromolecules 4, 1661–1668.

Ely, A., Baudu, M., Kankou, M.O.S.A.O., Basly, J.P., 2011. Copper and nitrophenol removal by low cost alginate/Mauritanian clay composite beads. Chem. Eng. J. 178, 168–174.

Escudero, C., Fiol, N., Villaescusa, I., 2006. Chromium sorption on grape stalks encapsulated in calcium alginate beads. Environ. Chem. Lett. 4, 239–242.

Escudero, C., Fiol, N., Villaescusa, I., 2009. Bollinger, Arsenic removal by a waste (hydr)oxide entrapped into calcium alginate beads. J. Hazard. Mater, 164.533-41.

Gorin, P.A.J., Spencer, J.F.T., 1966. Exocellular alginic acid from Azotobacter vinelandii. Can. J. Chem. 44, 993–998.

Gubin, S.P., Koksharov, Y.A., Khomutov, G.B., Yurkov, G.Y.E., 2005. Magnetic nanoparticles: preparation, structure and properties. Russ. Chem. Rev, 74.489-520.

Jagiello, J., Olivier, J.P., 2013. 2D-NLDFT adsorption models for carbon slit-shaped pores with surface energetical heterogeneity and geometrical corrugation. Carbon 55, 70–80.

Jagiello, J., Thommes, M., 2004. Comparison of DFT characterization methods based on N2, Ar, CO_2, and H_2 adsorption applied to carbons with various pore size distributions. Carbon, Carbon'03 Conf. 42, 1227–1232.

Kalfa, O.M., Yalçınkaya, Ö., Türker, A.R., 2009. Synthesis of nano B_2O_3/TiO_2 composite material as a new solid phase extractor and its application to preconcentration and separation of cadmium. J. Hazard. Mater., 166455-–461.

Kasperiski, M.F., Eder, C.L., Umpierres, S., Glaydson, S.R., Pascal, S.T., Diana, R.L., Silvio, L.P.D., Caroline, S., Janaina, D.C., 2018. Production of porous activated carbons from Caesalpinia ferrea seed pod wastes: highly efficient removal of Captopril from aqueous solutions. J. Clean. Prod. 197, 919–929.

Matricardi, P., Meo, C.D., Coviello, T., Alhaique, F., 2008. Recent advances and perspectives on coated alginate microspheres for modified drug delivery. Exp. Opin. Drug Deliv. 5, 417–425.

Ngomsik, A.F., Bee, A., Siaugue, J.M., Cabuil, V., Cote, G., 2006. Nickel adsorption by magnetic alginate microcapsules containing an extractant. Water Res. 40, 1848–1856.

Oladipo, A.A., Gazi, M., 2014. Enhanced removal of crystal violet by low cost alginate/acid activated bentonite composite beads: optimization and modelling using non-linear regression technique. J. Water Process Eng. 2, 43–52.

Painter, T.J., 1983. Algal polysaccharides. In: Aspinall, G.O. (Ed.), The Polysaccharides, 2. Academic Press, Orlando, FL, pp. 196–285.

Puttipipatkhachorn, S., Pongjanyakul, T., Priprem, A., 2005. Molecular interaction in alginate beads reinforced with sodium starch glycolate or magnesium aluminum silicate, and their physical characteristics. Int. J. Pharm. 293, 51–62.

Ramos, P.E., Silva, P., Alario, M.M., Pastrana, L.M., Teixeira, J.A., Cerqueira, M.A., Vicente, A.A., 2018. Effect of alginate molecular weight and M/G ratio in beads properties foreseeing the protection of probiotics. Food Hydrocolloid. 77, 8–16.

Rehman, I., Bonfield, W., 1997. Characterization of hydroxyapatite and carbonated apatite by photo acoustic FTIR spectroscopy. J. Mater. Sci.: Mater. Med. 8, 1–4.

Salah, A.A., Jozwiak, P., Zaghib, K., Garbarczyk, J., Gendron, F., Mauger, A., Julien, C. M., 2006. FTIR features of lithium-iron phosphates as electrode materials for rechargeable lithium batteries. Spectrochim. Acta. A. Mol. Biomol. Spectrosc. 65, 1007–1013.

Scott, D.C., Woodward, C.A., Thompson, J.E., 1989. Solute diffusion in biocatalyst gel beads containing biocatalysis and other additives. Enzyme Microb. Technol. 11, 258–263.

Silva, R.M.P., Manso, J.P.H., Rodrigues, J.R.C., Lagoa, R.J.L., 2008. A comparative study of alginate beads and an ion-exchange resin for the removal of heavy metals from a metal plating effluent. J. Environ. Sci. Heal. 43, 1311–1317.

Thu, B., Bruheim, P., Espevik, T., Smidsrød, O., Soon-Shiong, P., Skjåk-Bræk, G., 1996. Alginate polycation microcapsules: I. Interaction between alginate and polycation. Biomaterials 17, 1031–1040.

Umpierres, C.S., Thue, P.S., dos Reis, G.S., de Brum, I.A.S., Lima, E.C., de Alencar, W.A., Dias, S.L.P., Dotto, G.L., 2018. Microwave activated carbons from Tucum~ a (Astrocaryum aculeatum) waste for efficient removal of 2- nitrophenol from aqueous solutions. Environ. Technol., 391173-–1187.

Wenzel, H., Larsen, H.F., Clauson-Kaas, J., Høibye, L., Jacobsen, B.N., 2008. Weighing environmental advantages and disadvantages of advanced wastewater treatment of micro-pollutants using environmental life cycle assessment. Water Sci. Technol. 57 (1), 27–32.

Zhou, H., Smith, D.W., 2002. Advanced technologies in water and wastewater treatment. J. Environ. Eng. Sci, 4.247-264.